

# Naval Research Laboratory

Stennis Space Center, MS 39529-5004

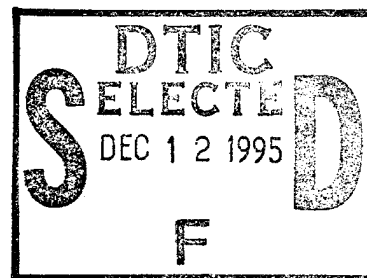


NRL/FR/7442--95-9630

## Applications of Hyperspectral Data in Coastal Marine Environments

GREGORY E. TERRIE

*Mapping, Charting, and Geodesy Branch  
Marine Geosciences Division*



November 17, 1995

19951208 072

Approved for public release; distribution is unlimited.

DTIC QUALITY INSPECTED 1

# REPORT DOCUMENTATION PAGE

Form Approved  
OBM No. 0704-0188

Public reporting burden for this collection of information is estimated to average 1 hour per response, including the time for reviewing instructions, searching existing data sources, gathering and maintaining the data needed, and completing and reviewing the collection of information. Send comments regarding this burden or any other aspect of this collection of information, including suggestions for reducing this burden, to Washington Headquarters Services, Directorate for Information Operations and Reports, 1215 Jefferson Davis Highway, Suite 1204, Arlington, VA 22202-4302, and to the Office of Management and Budget, Paperwork Reduction Project (0704-0188), Washington, DC 20503.

1. AGENCY USE ONLY (Leave blank)

2. REPORT DATE

November 17, 1995

3. REPORT TYPE AND DATES COVERED

Final

4. TITLE AND SUBTITLE

Applications of Hyperspectral Data in Coastal Marine Environments

5. FUNDING NUMBERS

Job Order No. 674566010

Program Element No. 0602435N

Project No. RO35S41

Task No.

Accession No. DN153129

6. AUTHOR(S)

Gregory E. Terrie

7. PERFORMING ORGANIZATION NAME(S) AND ADDRESS(ES)

Naval Research Laboratory  
Marine Geosciences Division  
Stennis Space Center, MS 39529-5004

8. PERFORMING ORGANIZATION  
REPORT NUMBER

NRL/FR/7442--95-9630

9. SPONSORING/MONITORING AGENCY NAME(S) AND ADDRESS(ES)

Naval Research Laboratory  
Oceanography Division  
Stennis Space Center, MS 39529-5004

10. SPONSORING/MONITORING  
AGENCY REPORT NUMBER

11. SUPPLEMENTARY NOTES

12a. DISTRIBUTION/AVAILABILITY STATEMENT

Approved for public release; distribution is unlimited.

12b. DISTRIBUTION CODE

13. ABSTRACT (Maximum 200 words)

The coastal environment is a highly dynamic region that is not understood very well, thus research efforts are underway to aid in the development of more accurate models that predict the optical properties of the water, determine bottom albedo, and develop methods for accurately measuring the environmental parameters needed by the models. The work presented in this thesis is in support of ongoing research by the Naval Research Laboratory using airborne hyperspectral imagery for the remote sensing of coastal environmental parameters. These research programs are intended to support the Navy's efforts in mine countermeasures, amphibious warfare, and shallow-water antisubmarine warfare.

14. SUBJECT TERMS

sensors, hydrography, bathymetry, optical properties, remote sensing, sediments

15. NUMBER OF PAGES

58

16. PRICE CODE

17. SECURITY CLASSIFICATION  
OF REPORT

Unclassified

18. SECURITY CLASSIFICATION  
OF THIS PAGE

Unclassified

19. SECURITY CLASSIFICATION  
OF ABSTRACT

Unclassified

20. LIMITATION OF ABSTRACT

Same as report

GRADUATE SCHOOL OF TULANE UNIVERSITY

APPLICATIONS OF HYPERSPECTRAL DATA IN  
COASTAL MARINE ENVIRONMENTS

By  
Gregory E. Terrie

A THESIS

Submitted to the Department of Electrical Engineering  
of the Graduate School of Tulane University  
in partial fulfillment of the requirements for  
the degree of Master of Science

New Orleans, Louisiana

July, 1995

Accession For	
NTIS CRA&I	<input checked="" type="checkbox"/>
DTIC TAB	<input type="checkbox"/>
Unannounced	<input type="checkbox"/>
Justification	
By	
Distribution/	
Availability Codes	
Dist	Avail and/or Special
A-1	

## SUMMARY

The coastal environment is a highly dynamic region that is not understood very well, thus research efforts are underway to aid in the development of more accurate models that predict the optical properties of the water, determine bottom albedo, and develop methods for accurately measuring the environmental parameters needed by the models. The work presented in this thesis is in support of ongoing research by the Naval Research Laboratory using airborne hyperspectral imagery for the remote sensing of coastal environmental parameters. These research programs are intended to support the Navy's efforts in mine countermeasures, amphibious warfare, and shallow-water antisubmarine warfare.

## ACKNOWLEDGMENTS

This work was supported by the Naval Research Laboratory, Hyperspectral Characterization of the Coastal Environment, Program Element RO35S41, Dr. Herbert C. Eppert, Jr., Project Manager, and Littoral Optical Environment, ONR Program Element 0602435N, Robert Feden, Program Manager. The author wishes to thank the thesis committee, especially Dr. Andrew Martinez; Dr. Charles Walker for guidance throughout this effort; Ms. Maria Kalcic, Dr. Robert Arnone, Dr. Richard Gould, and Dr. Alan Weideman for their technical recommendations; and Mr. Michael Harris and Dr. Edward Mozley for their encouragement and support throughout this process.

# APPLICATIONS OF HYPERSPECTRAL DATA IN COASTAL MARINE ENVIRONMENTS

A THESIS

SUBMITTED THE FOURTEENTH DAY OF JULY, 1995

TO THE DEPARTMENT OF ELECTRICAL ENGINEERING

OF THE GRADUATE SCHOOL OF

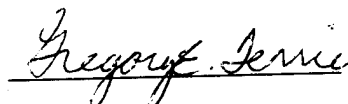
TULANE UNIVERSITY

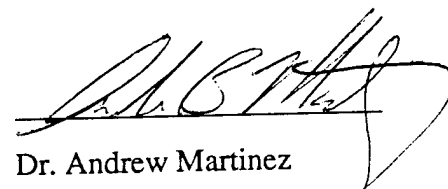
IN PARTIAL FULFILLMENT OF THE REQUIREMENTS

FOR THE DEGREE OF


MASTER OF SCIENCE

BY

  
GREGORY E. TERRIE

  
Dr. Andrew Martinez


Chairman

  
Dr. Paul Duvoisin

Dr. Paul Duvoisin

  
Dr. G. Lee Zimmerman

Dr. G. Lee Zimmerman

  
Dr. Charles Walker

Dr. Charles Walker

## Abstract

High resolution spectral data collected during field exercises at Eglin Air Force Base, near Fort Walton Beach, Florida, during August 1994 are presented to demonstrate the usefulness of this type of data for estimating the reflectance of land and water features in a coastal marine environment. The data consists of spectral imagery collected by the Compact Airborne Spectrographic Imager (CASI) and *in-situ* spectral data measured by the Analytical Spectral Devices, Inc. VNIR FieldSpec (ASD).

A remote sensing reflectance model is used to compute water reflectance from the CASI and ASD data. The good agreement between the CASI and ASD results suggest that airborne and eventually spaceborne hyperspectral sensors can be used to measure water reflectance. The spectral reflectance signatures of several land features found at the Eglin test site demonstrate that hyperspectral data is a valuable tool for distinguishing between features. Principal component analysis is also used in an effort to reduce the dimensionality of the hyperspectral data. The results show that, for both the CASI and ASD data, over 90% of the variability of the data is contained in the first two principal components. The data analysis procedures developed to process both the CASI and ASD data are also presented.

## Table of Contents

Chapter 1 INTRODUCTION.....	1
Chapter 2 BACKGROUND .....	5
2.1 Theory .....	5
2.2 Model .....	14
2.3 Principal Component Analysis.....	15
Chapter 3 PROCEDURES .....	19
3.1 Statement of Problem.....	19
3.2 Data Collection.....	20
3.3 Data Processing and Analysis .....	23
Chapter 4 RESULTS.....	29
Chapter 5 CONCLUSIONS AND RECOMMENDATIONS .....	45
References .....	49



## **Chapter 1**

### **Introduction**

The purpose of this paper is to demonstrate the suitability of high resolution spectral data for remote sensing of coastal environmental parameters. The spectral data presented in this paper was collected during August 1994 at Eglin Air Force Base near Fort Walton Beach, Florida. The data consists of hyperspectral imagery from the Compact Airborne Spectrographic Imager (CASI) and high resolution spectra collected *in-situ* using the hand held Analytical Spectral Devices, (ASD) Inc. VNIR FieldSpec.

The major results of this thesis show that CASI spatial mode imagery can be used to measure remote sensing reflectance of the water in a coastal marine environment. The reflectance of the water was found to be less than 5%, which is within the expected range. The hyperspectral reflectance signatures of land features also demonstrate that this type of data can be used to distinguish between other features, including the water. Principal component analysis (PCA) was also used to reduce the dimensionality of the hyperspectral data. Over 90% of the variation in the data is contained in the first two principal components. Although the PCA results are not completely understood, they are intriguing, thus further research with this technique is definitely warranted.

Optical remote sensing instruments are categorized as either passive or active. An active sensor detects the reflected light from its own light source. An airborne laser

system used for measuring bathymetry is an example of an active remote sensor. In contrast, passive remote sensors detect the amount of sunlight reflected from the earth's surface. CASI is an example of a passive remote sensor. These sensors separate the reflected light into a number of spectral channels or bands that span the visible and infrared portion of the electromagnetic spectrum. The number of bands and the spectral coverage varies from sensor to sensor. Multispectral imaging (MSI) sensors, such as the LANDSAT satellite, have only a few bands; usually less than 10. Other sensors, such as, CASI and the Airborne Visible-Infrared Imaging Spectrometer (AVIRIS), have hundreds of narrow bands and are referred to as hyperspectral imaging (HSI) sensors.

MSI and HSI sensors have been used in a variety of applications ranging from global environmental monitoring, mapping, charting, geodesy, land use planning, natural resource management, water quality monitoring, oceanography, and wildlife habitat management. and are being used to collect imagery in the coastal maritime environment. Most of these sensors, however, were originally designed and optimized for use over land. The one notable exception is the Coastal Zone Color Scanner (CZCS) which was designed specifically for measurement of the optical properties of the world's oceans.

The application of high resolution spectral data in a coastal marine environment is the focus of this paper. Researchers have used both MSI and HSI sensors to extract environmental parameters, such as, water clarity, chlorophyll concentration, particulate and biological absorption and scattering, bathymetry, bottom reflectance and suspended sediment concentrations [3,7,9,13,14]. The problem that usually exists with using most

MSI sensors in the maritime environment is the lack of adequate spectral coverage in the blue and green portions of the visible spectrum. These wavelengths contain the important absorption and reflectance bands for detecting chlorophyll and other biological matter. Additionally, the blue and green wavelengths penetrate deeper into the water and are useful for bathymetry and bottom characterization. As a consequence of their high spectral resolution, the HSI sensors provide more than adequate spectral coverage throughout the visible spectrum. Additionally, by resampling of both the pixel size and channel bandwidth of HSI data, unaliased simulations of other current and future MSI and HSI sensors can be performed.

The lack of reliable high resolution data in coastal areas has hampered coastal optics model development. The lack of data is due in part to the costly and time consuming method of *in-situ* measurements by ship. The advantages of using airborne or satellite remote sensors to collect data versus ship measurements are rather obvious. For instance, remote sensors can collect data at a faster rate, with high spatial resolution, and with the capability of a shorter time between revisits. Remote sensors are also capable of collecting data in areas where access is denied by foreign countries.

Increased measurement and modeling research by government, university, and private sector groups has begun in order to address the need for a better understanding of the coastal environment. The Department of Defense (DOD) is placing more emphasis on regional conflicts, such as the Persian Gulf War, since the perceived threat from deep ocean submarines has decreased due to the end of the Cold War. The US Navy has

refocused efforts from deep ocean scenarios to the littoral scenario, which encompasses the coastal environment. Understanding the coastal environment is vital to the successful planning and execution of Naval operations. Reduced research budgets in all sectors has led to joint research efforts between DOD, NASA, NOAA, university, and private sector organizations. By combining resources researchers are provided opportunities to collect coincident and comprehensive data that include MSI, HSI, and the necessary *in-situ* measurements that are needed in the development of coastal optics models. The data presented in this paper was collected as part of a joint DOD research project.

The layout of this paper is as follows. Chapter 2 will provide the background information including recent research using HSI sensors in coastal areas, as well as, a summary of the remote sensing reflectance model used in this paper. Chapter 3 describes the data collected during the Eglin field exercises and gives a description of how the data was analyzed. The results are provided in Chapter 4, followed by the conclusions and recommendations in Chapter 5.

## **Chapter 2**

### **Background**

The purpose of this chapter is to provide a brief overview of previous research conducted using passive optical remote sensing instruments for studying the maritime environment. A summary of the remote sensing reflectance model used in this paper will be presented, as well as background information on principal component analysis (PCA). The information provided in this chapter is by no means exhaustive. The reader is encouraged to obtain the references cited below for more detailed information.

#### **2.1 Theory**

An in-depth presentation of the physics that models the path of sunlight as it travels from the top of the atmosphere, to the earth's surface, its interaction with the ocean, and its return back through the atmosphere to the detectors of the remote sensing instrument is beyond the scope of this work. A collection of papers consolidated by Jerlov [1] and Tyler [2] give an overall view of optical oceanography and the physics of light in sea water. In general, the remote sensing instrument detects the amount of sunlight that is reflected by features on the earth's surface. As depicted in Figure 1, the sunlight first must travel through the atmosphere where the light is either scattered by molecules (Rayleigh) or aerosols, or is absorbed by ozone, oxygen, water vapor, or other gases. The air-water interface further attenuates the light according to the Fresnel reflection coefficient of

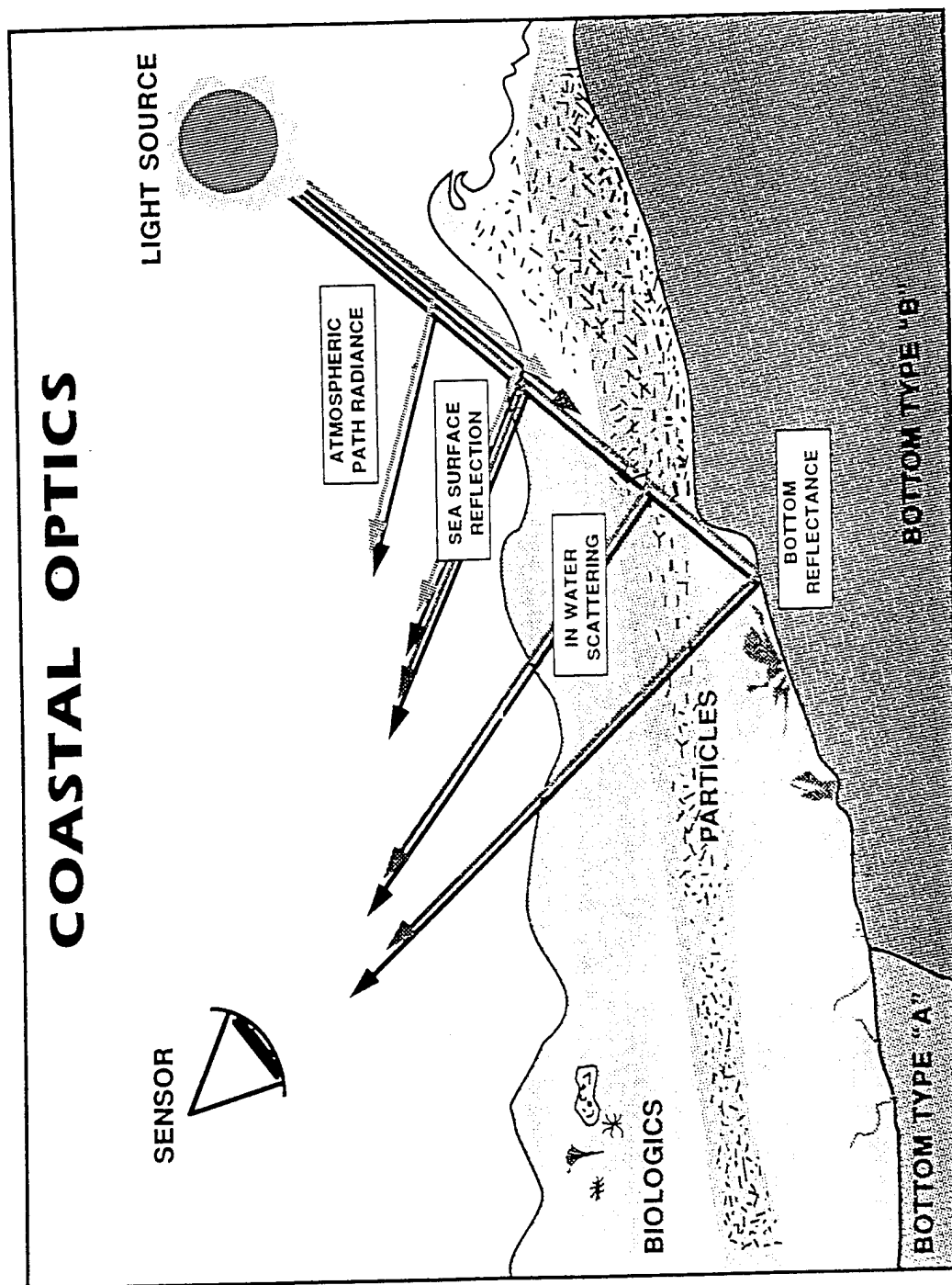


Figure 1: Depiction of absorption and scattering of sunlight in a coastal marine environment.

water. Once in the water, the light again encounters absorption and scattering. The water itself, along with pigments in photosynthetic plant material and colored dissolved organic material (CDOM) are responsible for a majority of the absorption. In the turbid coastal areas, scattering is attributed to suspended sediments and biological particulates. In shallow areas the bottom affects the light by reflection or absorption.

The use of satellite or airborne MSI for monitoring of the ocean environment is not a new concept. The Coastal Zone Color Scanner (CZCS) was the first satellite ocean color sensor with four bands in the visible and one in the near-infrared [5]. Researchers have used CZCS data to study the relationships between physical processes, watermass variability, and photosynthetic productivity in the ocean. For instance, Gordon et al. [6] related CZCS estimates of chlorophyll concentrations to the turbidity of the water (diffuse attenuation coefficient). Austin and Petzold [7] used the power law of spectral radiance ratios to relate CZCS radiance to the diffuse attenuation coefficient. Arnone et al. [8] developed a world-wide CZCS ocean color database, at 20km spatial resolution, capable of providing climatological estimates of the water optical properties. A follow-on satellite to the defunct CZCS, SeaWiFS has been developed, however, the launch date has been postponed. Notwithstanding the important contributions of CZCS, and potentially SeaWiFS, to the understanding of physical processes in the ocean environment, these instruments are not suitable for some applications, particularly Naval operations, in the near-shore coastal environment due the rather coarse spatial resolution (approximately 1km for CZCS), and limited spectral range. The coastal environment typically consists of land features as well which are consequently masked out by both CZCS and SeaWiFS.

LANDSAT, with its seven spectral bands, four visible, one near-IR, one mid-IR and one thermal, was primarily designed for use over land, however, it has been used to measure maritime environmental parameters, such as bathymetry and bottom type. Algorithms for extracting bathymetry from MSI have been proposed by several authors [9,10,11]. These algorithms are based on a simple water reflectance model given by

$$L_i = L_{\infty i} + c_i R_{ai} e^{-2k_i z} \quad (1)$$

$L_i$  is the radiance received by the remote sensor for band  $i$ ,  $L_{\infty i}$  is the deep-water radiance due to external reflection of the sea surface, atmospheric scattering, and water volume scattering,  $c_i$  is a constant attributed to solar irradiance, atmospheric and sea surface transmittance and sea surface refraction,  $R_{ai}$  is the bottom reflectance,  $k_i$  is the effective attenuation coefficient of the water, and  $z$  is the water depth. Estimating sediment concentration [12] and sediment transport [13] are other applications of LANDSAT data.

Hyperspectral sensors, such as AVIRIS, have also been used to study the coastal environment. AVIRIS has 224 narrowly spaced spectral channels ranging from 400nm to 2400nm. AVIRIS also was originally developed for use over land, however, due to its high spectral (9.5 nm) and spatial (20m) resolution it is being used as a testbed for ocean optics algorithm development. Its narrow channels also allow researchers to produce unaliased simulations of many of the current and future imaging sensors. Carder et al. [14] and Hamilton et al. [15] demonstrate the use of AVIRIS data in computing water optical properties, such as reflectance, absorption, and chlorophyll content.



Analyzing spectral data in marine environments is much more challenging than in geologic or vegetative areas. Due to the exponential increase in light attenuation in the red wavelengths, most ocean optics research is limited to the visible spectrum in the 400nm to 700nm range. Additionally, the reflectance of water targets are on the order of only 2% to 7%, whereas the reflectance of land targets range 10% to 50% or higher. A typical coastal scene might contain land features, such as, beach sand, grass, roads, trees, etc., in addition to the water. Therefore, the remote sensing instrument must have both adequate signal-to-noise ratio (SNR) and dynamic range in order to accommodate the wide range of reflectances that may be encountered.

Hamilton et al. [15] used AVIRIS data over Lake Tahoe to estimate chlorophyll content and compared those results to *in-situ* measurements. The clear waters of Lake Tahoe closely match those of the clearest ocean waters. The CZCS chlorophyll algorithm developed by Gordon et al. [6], was used to compute chlorophyll concentration from the AVIRIS data. There was good agreement between the AVIRIS estimated chlorophyll concentration and the *in-situ* measurement. However, poorer results were obtained at other locations. The authors attributed the error to the covarying absorption of CDOM with chlorophyll at 440 nm, which the model could not correct for, and inaccurate calibration of AVIRIS in the blue wavelengths. The paper also showed that AVIRIS derived upwelling radiance ( $L_w$ ) agreed very well with *in-situ* measurements as shown in Figure 2. Additionally, the authors pointed out that since AVIRIS lacks the SNR, especially in the blue, to resolve changes in photosynthetic pigments, thus spatial averaging is necessary. Pilorz and Davis [16] indicated that a SNR of 95, including

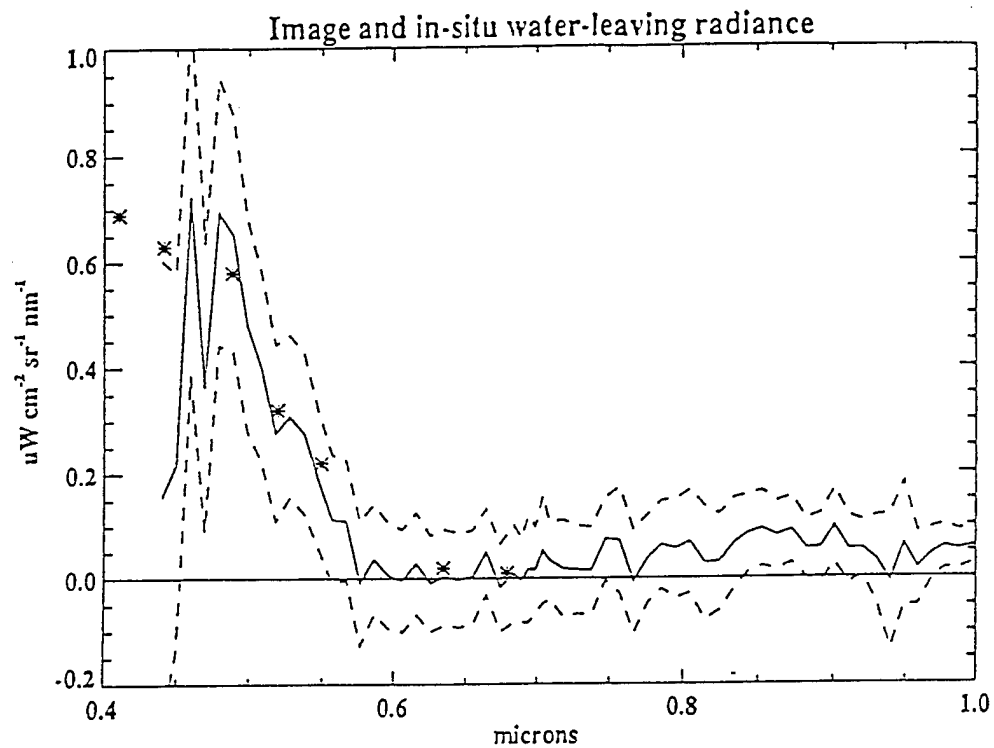


Figure 2: Comparison of the water-leaving radiance measured using the AVIRIS, and the same quantity derived by propagating in-water measurements to just above the surface (discrete points). [Figure 8 from Hamilton et al. 1993].

atmospheric effects, was needed to detect changes chlorophyll concentration on the order of  $1 \text{ mg m}^{-3}$ .

Carder et al. [14] compared remote sensing reflectance ( $R_{rs}$ ), derived from AVIRIS imagery, with *in-situ* measurements. Spatial averaging was also used to increase SNR. Additionally, the authors used a post-flight recalibration scheme to improve the sensitivity of the sensor, particularly in the shorter wavelengths. Figure 4 illustrates the good agreement between the AVIRIS measured  $R_{rs}$  and the *in-situ* measurements. The paper also uses the models described by Lee et al. [4] to quantify the components of  $R_{rs}$ . For instance, Figure 3 compares AVIRIS measured  $R_{rs}$  with modeled results of  $R_{rs}$ , remote sensing reflectance due to bottom reflectance ( $R_{rsb}$ ), and reflectance of the water from scattering due to molecules and particles ( $R_{rsw}$ ). A deep-to-shallow transect illustrating spectral changes due to changes in depth is shown in Figure 5.

The upwelling light sensed by passive spectral sensors contains a mixture of all of the absorption and scattering effects of the constituents present in the water. No reliable procedures have been developed to unmix these effects from water spectra. An abundance of geological applications exist which use linear and non-linear spectral unmixing algorithms to identify and determine the relative abundances of components in mixed reflectance spectra. For example, Kruse et al. applied linear spectral unmixing techniques to the mapping of minerals using AVIRIS [18], while Huete and Escadafal [19] used linear unmixing techniques to characterize soil spectral signatures from LANDSAT data. Some water applications do exist, most notably in the area of suspended sediments. Mertes et al. [13] used unmixing techniques to estimate suspended sediment

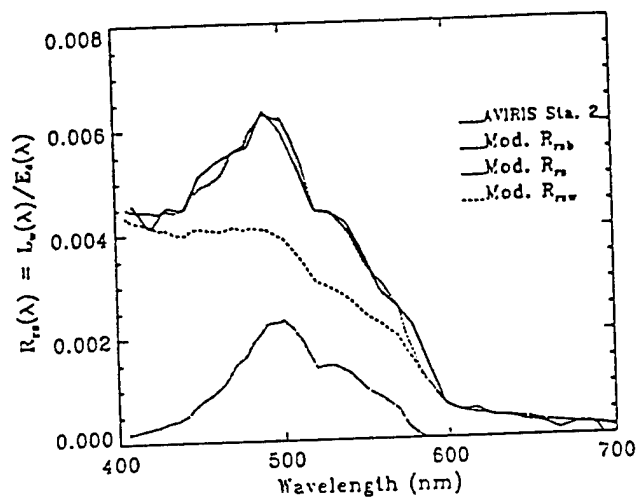


Figure 3:  $R_{rs}(\lambda)$  spectra from AVIRIS and a model for Station 2. The contributions attributed to bottom reflection (MOD.  $R_{rsb}$ ) and water-column reflectance (MOD.  $R_{rsw}$ ) are shown separately. [Figure 4a from Carder et al. 1993].

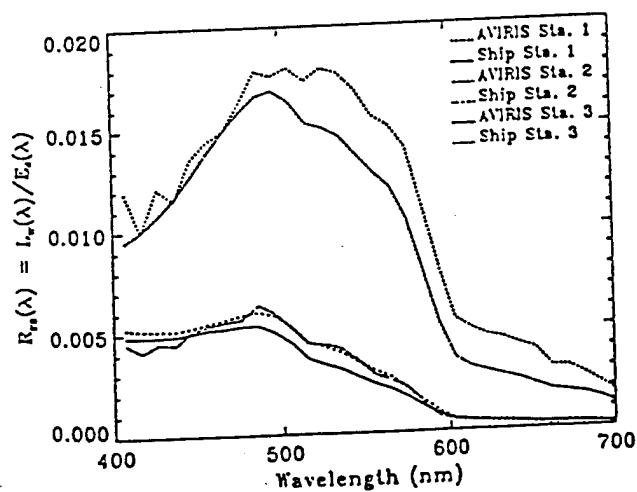


Figure 4: Comparison of  $R_{rs}(\lambda)$  spectra from AVIRIS and *in-situ* data. [Figure 3 from Carder et al. 1993].

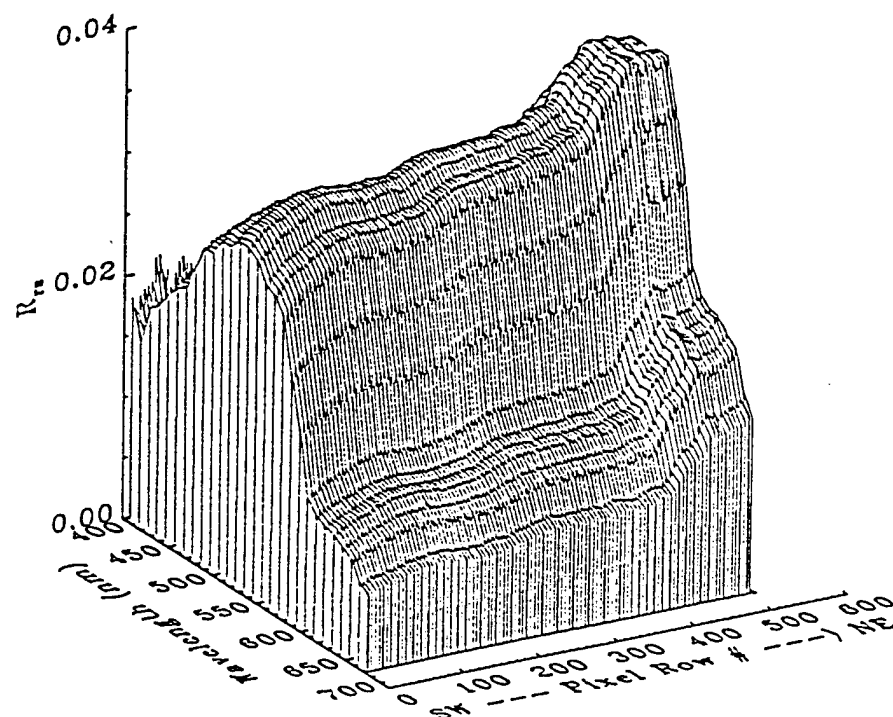


Figure 5: Row averaged spectra of  $R_n(\lambda)$  from AVIRIS. Each row is 20m wide. [Figure 5 from Carder et al. 1993].

concentrations from LANDSAT data. In these applications, it is assumed that a mixed spectra can be modeled as a linear combination of pure members of an endmember library.

## 2.2 Model

The light detected by the remote sensor depicted in Figure 1 is a combination of the effects from the atmosphere, water, and bottom. The total radiance detected by the sensor, from Gordon and Clark [3], can be expressed as

$$L(\lambda) = L_r(\lambda) + L_a(\lambda) + t(\lambda) L_w(\lambda), \quad (2)$$

where  $L_r(\lambda)$  is the radiance due to Rayleigh scattering,  $L_a(\lambda)$  is the radiance due to aerosol scattering,  $L_w(\lambda)$  is the water leaving radiance, and  $t(\lambda)$  is the atmospheric diffuse transmission. Lee et al. [4] show that  $L_w(\lambda)$  can be expressed by a sum of its components

$$L_w(\lambda) = L_w^w(\lambda) + L_w^b(\lambda) + L_w^f(\lambda) + L_w^R(\lambda), \quad (3)$$

where  $L_w^w(\lambda)$  is the radiance from scattering due to molecules and particles,  $L_w^b(\lambda)$  is the radiance from bottom reflectance,  $L_w^f(\lambda)$  is the radiance due to CDOM fluorescence, and  $L_w^R(\lambda)$  is the radiance due to Raman scattering.

In order to remove the implied solar contribution in Equation (2), remote sensing reflectance, defined to be the ratio of the upwelling radiance to the above surface irradiance, and given by

$$R_{rs} = \frac{L_w}{E_d(0^+)}, \quad (4)$$

can be used instead. For clarity, the wavelength dependence, although not indicated, is assumed.  $R_{rs}$  is also expressed as a sum of its components as shown by

$$R_{rs}(\lambda) = R_{rs}^w(\lambda) + R_{rs}^b(\lambda) + R_{rs}^f(\lambda) + R_{rs}^R(\lambda). \quad (5)$$

Equation (4) forms the basis for most of the computations applied to the spectral data presented in this paper. The reflectance spectra can be used to distinguish between the many different features found in the coastal environment.

### 2.3 Principal Component Analysis

Principal component analysis (PCA) is known by a variety of other names, such as the eigenvector analysis, the Hotelling transform, or discrete Karhunen-Loève transform. PCA is based on the statistical properties of vector representations. An outline of the pertinent equations will be provided in this section. A more detailed discussion of this technique is described in [21], and [22].

Hyperspectral data provides many additional bands across the entire electromagnetic spectrum. The spectral range between 400 nm and 700 nm is of primary importance to the oceanographic community. CASI has 170 bands and the ASD instruments have 210 bands within that range. Dealing with 200 or so bands is messy and cumbersome to say the least. PCA was chosen to attempt to reduce the number of bands needed in processing both the CASI and ASD spectral data in a systematic manner, yet maintaining the variability within the data.

The spectra collected either by CASI or ASD can be considered as a population of random spectra of the form

$$\mathbf{x} = \begin{bmatrix} x_1 \\ x_2 \\ \vdots \\ x_n \end{bmatrix} \quad (6)$$

The mean of the population is  $\mathbf{m}_x = E\{\mathbf{x}\}$ . The covariance matrix of the population is defined as

$$\mathbf{C}_x = E\{(\mathbf{x} - \mathbf{m}_x)(\mathbf{x} - \mathbf{m}_x)^T\} \quad (7)$$

Note that  $\mathbf{C}_x$  is a square matrix of size  $n \times n$ . Element  $c_{ii}$  is the variance of  $x_i$ , the  $i$ th band of the spectra and  $c_{ij}$  is the covariance between bands  $i$  and  $j$ . The covariance matrix is real and symmetric. Assume that there are  $M$  sample spectra from the random population of spectra. The mean and covariance matrix for the population can be approximated from the samples by

$$\mathbf{m}_x = \frac{1}{M} \sum_{k=1}^M \mathbf{x}_k \quad (8)$$

and

$$\mathbf{C}_x = \frac{1}{M} \sum_{k=1}^M \mathbf{x}_k \mathbf{x}_k^T - \mathbf{m}_x \mathbf{m}_x^T \quad (9)$$

By definition, the eigenvectors and eigenvalues of  $\mathbf{C}$  satisfy the relation

$$\mathbf{C}\mathbf{e}_i = \lambda_i \mathbf{e}_i, \text{ for } i = 1, 2, \dots, n. \quad (10)$$



If  $A$  is a matrix whose columns are formed from the eigenvectors of  $C_x$  ordered such that the first column of  $A$  is the eigenvector corresponding to the largest eigenvalue and the last column of  $A$  is the eigenvector corresponding to the smallest eigenvalue.  $A$  is known as the principal component matrix which can be used to transform by

$$y = A^T(x - m_x) \quad (11)$$

The elements of  $y$  are uncorrelated. Furthermore,  $C_y$  has the same eigenvalues and eigenvectors of  $C_x$ . Any  $x$  can be recovered from its corresponding  $y$  by the equation

$$x = Ay + m_x \quad (12)$$

Since  $A$  is has orthonormal rows  $A^{-1} = A^T$ . Equation (12) can be used to estimate by using only the first  $K$  eigenvectors corresponding to the first  $K$  largest eigenvalues. The estimated  $x$  vector is given by

$$\hat{x} = A_K y + m_x \quad (13)$$

The mean square error (MSE) is given by

$$MSE = \sum_{j=K+1}^n \lambda_j \quad (14)$$

Thus, by using the  $K$  largest eigenvalues, the mean square error is minimized between  $x$  and  $\hat{x}$ .

The reason for using PCA for the spectral data is to hopefully find a reduced number of uncorrelated parameters that represents the original spectra within some tolerable MSE. Ideally, it would be extremely useful to be able to associate each of the

principal components with some physical phenomenon (i.e. brightness, bathymetry, water clarity, etc).

## **Chapter 3**

### **Procedures**

The data processing and analysis procedures described in this chapter were developed specifically to process both the ASD and CASI data for the Eglin field exercises held during August 1994.

#### **3.1 Statement of Problem**

One of the goals of this thesis is to determine the reflectance of the water, in a coastal marine environment, using airborne hyperspectral data collected by the CASI sensor and compare it to ground truth data in the form of high resolution spectral data using the Analytical Spectral Devices (ASD), Inc. VNIR FieldSpec. Additionally, the hyperspectral reflectance signature of a feature (i.e. sand, water, vegetation, etc.) found in the coastal environment can be used to distinguish it from other features. The reflectance is an important property of a feature since it is independent of illumination and is dependent upon the physical and chemical composition of the feature.

The coastal marine environment is not well understood is much more complex than the open ocean due to the presence of dissolved and particulate matter which have varying absorption, scattering, and fluorescence properties, as well as, influences due to varying bottom type and bathymetry. The upwelling radiance and ultimately the spectral

reflectance detected by the passive remote sensor is a combination of all of these absorption and scattering effects within the water column and on the bottom. Previous multispectral data sources, like CZCS, provided valuable information on ocean optical properties, however, its large spatial resolution, 800m, would be undesirable for nearshore environments. The future of the multispectral SeaWiFS instrument, the CZCS follow-on, is unclear, therefore, ocean color researchers, in the meantime, will have to rely on airborne HSI sensors to provide data for model development. This paper does not attempt to develop any new models. Instead the remote sensing reflectance model described in Chapter 2 is used.

### 3.2 Data Collection

The CASI instrument is one of 19 known airborne hyperspectral sensors either available now or in the near future [17]. Table 1 [17] provides a brief summary of the characteristics of the known hyperspectral sensors. The CASI sensor, developed by ITRES Research Ltd. and flown by Borstad Associates, is a lightweight, portable, pushbroom scanner controlled by a 386 PC that can be flown in a variety of small aircraft. CASI was flown in a Cessna 172 aircraft at altitudes ranging from 1100 ft to 10000 ft during the Eglin field exercises. Pushbroom scanners collect imagery by scanning a line at a time perpendicular to the motion of the aircraft (across-track). The forward motion of the aircraft allows the sensor to sweep a swath of data along track, thus forming an image. CASI has two different modes of operation: spatial and spectral.

SYSTEM	RANGE (nm)	BAND- WIDTH (nm)	CHANNELS	IPOV (mrad)	FOV	PIXEL/ LINE	DIGITL ZATION	DATA STORAGE	PLATFORMS
AAHIS-1	440-835	11	36 72	1.0	193 mrad	193	12 bit	Mac/Quadra 800, 1.2 GB hard drive, 5.0 GB Exabyte tape	Piper Aztec
AHS	#1 430-830 #2 1605-2405 #3 3000-5400 #4 8200-12700	20 50 300 400-1500	20 15 7 6	2.5	85.92°	715	12 bit	Serial to VLDS	NASA/ARC C-130, ER2, ERJM, Canbou
AIS	#1 400-1050 #2 1080-1800 #3 2000-2500	25.4 102 15.6	24 7 32	2.5-4.5	90°	512-1024	16 bit	9-track CCT	Piper Aztec, Piper Navajo
AMSS	#1 400-1050 #2 2050-2400 #3 8500-12000	20 44 530	32 8 8	2.1 x3	92.16°	768	8 bit	Winchester disks, 600MB optical disks	Light Aircraft
ASAS	420-1037	11	62	0.7	19°	512	12 bit	VLDS	NASA Wallops Island P-3B, NASA/ARC C-130
AYIRIS	400-2500	10	224	1.0	30°	614	12 bit	HDT, 10GB	NASA/ARC ER-2, Altitude 20,000m
CASI	430-870	3.0	<38	1.2	35.4°	578	12 bit	Exabyte 8500 8mm Helical Scan	Helicopter, Light Aircraft, Zeiss Camera Port
CHRSS	425-850	3.4	125	0.17-0. 5	10.3°	1024		Digital/Analog Data	Fixed Wing, Helicopter, UAV
DAIS-2815	#1 700-1000 #2 3000-5000 #3 8000-12000	300 600 200	1 3 20	1.0 2.5 5	82°	512-2048	15 bit	IBM 3480	Piper Navajo
DAIS-7915	#1 400-1000 #2 1000-1800 #3 1970-2450 #4 3000-5000 #5 8000-12300	16 100 16 2000 600	32 8 32 1 6	1.1 2.2 3.3	78°		16 bit	IBM 3480 Cartridge	Piper Navajo
HYDICE	400-2500	3.1 min., 14.9 max., 10.2 avg.	206	0.5	8.94°	312	12 bit		Altitude C141, up to 14,000m
MIVIS	#1 430-830 #2 1150-1550 #3 2000-2500 #4 8200-12700	20 50 8 400-500	20 8 64 10	2.0	72°	755	12 bit	Serial to VLDS	Aerial Survey Craft
MUSIC	#1 2500-7000 #2 6000-14500	25-70 60-1400	90 90	0.5	1.3° swath width x 2.6°	45	80 frames/s digital PCM		Canberra, U2
ROSI	430-880	5	256	0.55	±16°	512	12 bit	Digital Recorder	Jet Aircraft
SMIFTS	1.0-5.2µm		100	0.66	9.7°	256	12 bit		Helicopter
TRWIS-B	0.46-0.88µm	4.8	90	1	14°	± 240	8 bit	VHS	Helicopters, Light Aircraft
TRWIS-SC	0.46-0.88µm	4.8	90	1	60°	1000	8 bit	VHS	Helicopters, Light Aircraft
TRWIS-II	1.5-2.5µm	12	85	.5/1	7/14°	240	8 bit	VHS	Helicopters, Light Aircraft
WIS (unoccupied)	0.4-0.6µm 0.6-1.0µm 1.0-1.8µm 1.8-2.5µm	12.5 6 30 12.5	17 67 27 45	0.65	20°	512	12 bit	Hard Disk	Light Aircraft

Table 1: Hyperspectral Sensor Specifications. [Table 1 from Birk and McCord 1994].

In the spatial mode, CASI operates similar to other pushbroom imagers by collecting high resolution spatial imagery simultaneously in up to fifteen programmable bands. In spectral mode, CASI collects high resolution spectral information in 288, 1.8nm bands. Data is not collected across the entire swath, but in one or more user selectable spectral columns, called "look directions", across the swath. The spectral mode also provides a coregistered monochromatic high spatial resolution reference image which is formed from data from the "track recovery row". The purpose of the reference image is for target location and spatial orientation for the spectral data. Unlike AVIRIS, which collects full spectral and spatial data simultaneously, the CASI operating modes do not operate simultaneously.

The spatial resolution of CASI varies according to altitude, airspeed, and sensor integration or exposure time. In general, the across track and along track resolutions are not the same, therefore, the data is spatially resampled in order to obtain square pixels. The spatial resolution of the CASI data collected at Eglin ranged from about 2.5m to 4m. In spectral mode, the along track resolution was on the order of 10m.

The ASD instrument was used to measure the spectral reflectance of various land and water targets. The instrument is comprised of a 512 plasma coupled photodiode array, controlled by a 486 notebook computer. Input to the spectrometer is via a 1m fiber optic cable with a pistol grip attachment. An 18° field-of-view (FOV) tube to restrict the field of view was attached to the end of the pistol grip. The ASD has 512, 1.4nm bands in the range from 350nm to 1100nm. Integration time is manually selectable with a range

from 16 ms to 4 minutes. The 486 notebook computer also provides real-time display and storage of the measured spectra.

During the Eglin field exercises, CASI was flown at various altitudes, in both spatial and spectral mode, twice daily. Using two identically equipped ASD instruments, *in-situ* spectra at various stations, both in water and on land, were measured concurrently with the CASI overflights. While one of the ASD instruments made measurements at sea, the other instrument made simultaneous measurements of the reference target and the sky. Using the ASD instruments in tandem reduced the measurement load of the instrument at sea. As each ASD measurement was made, ancillary information, such as target description, sky conditions, reference target used, integration time, and output filename, were recorded on log sheets.

The CASI spatial data was roll and pitch corrected, georeferenced, and radiometrically calibrated by Borstad Associates prior to delivery. The spatial data was resampled so that the final pixel size was square. The only pre-processing performed on the spectral data by Borstad Associates was to convert the data to radiance values. The ASD instruments were not radiometrically calibrated, thus only raw digital counts were available. Since reflectance is the ultimate output, radiometric calibration of the ASD instruments, although desirable, is not really necessary.

### **3.3 Data Processing and Analysis**

The data processing software developed to analyze the ASD and CASI data was a combination of code written in C, Interactive Data Language (IDL), and MATLAB, all of

which was developed specifically for this project. The data was processed using a SUN SPARC2 UNIX workstation and a 486 PC.

Each ASD spectra is stored in a binary file comprised of a 484 byte header block, which contains information pertaining to the state of the instrument at the time that the spectra was saved, followed by the actual spectral data. The header information that was important to the data processing included the integration time, dark current correction flag, and time stamp. The dark current is the amount of current due to heat added to the detector output, which varied with time and temperature. Spectra without the dark current correction were not used.

Over 1500 ASD spectra were collected during the Eglin field experiment. In order to document all of the spectra taken, a program, written in IDL, was developed that each spectra along with the header information mentioned in the previous paragraph. The program prints nine spectra to a page as illustrated by Figure 6. This hardcopy log of the spectra becomes invaluable during data processing because it provides an efficient method in which to examine each spectra and correlate the header information with the log sheets.

Since the values of the ASD spectra were in units of digital counts, each spectra was normalized by its respective integration times prior to use in any of the calculations. Using the procedure described by Hamilton et al. [15], the ASD spectra were used to compute  $R_{rs}$  in Equation (4) using the formula

$$R_{rs} = \frac{S_{w+rs} - S_s \rho(\theta)}{(\pi S_g / r_g)} . \quad (15)$$



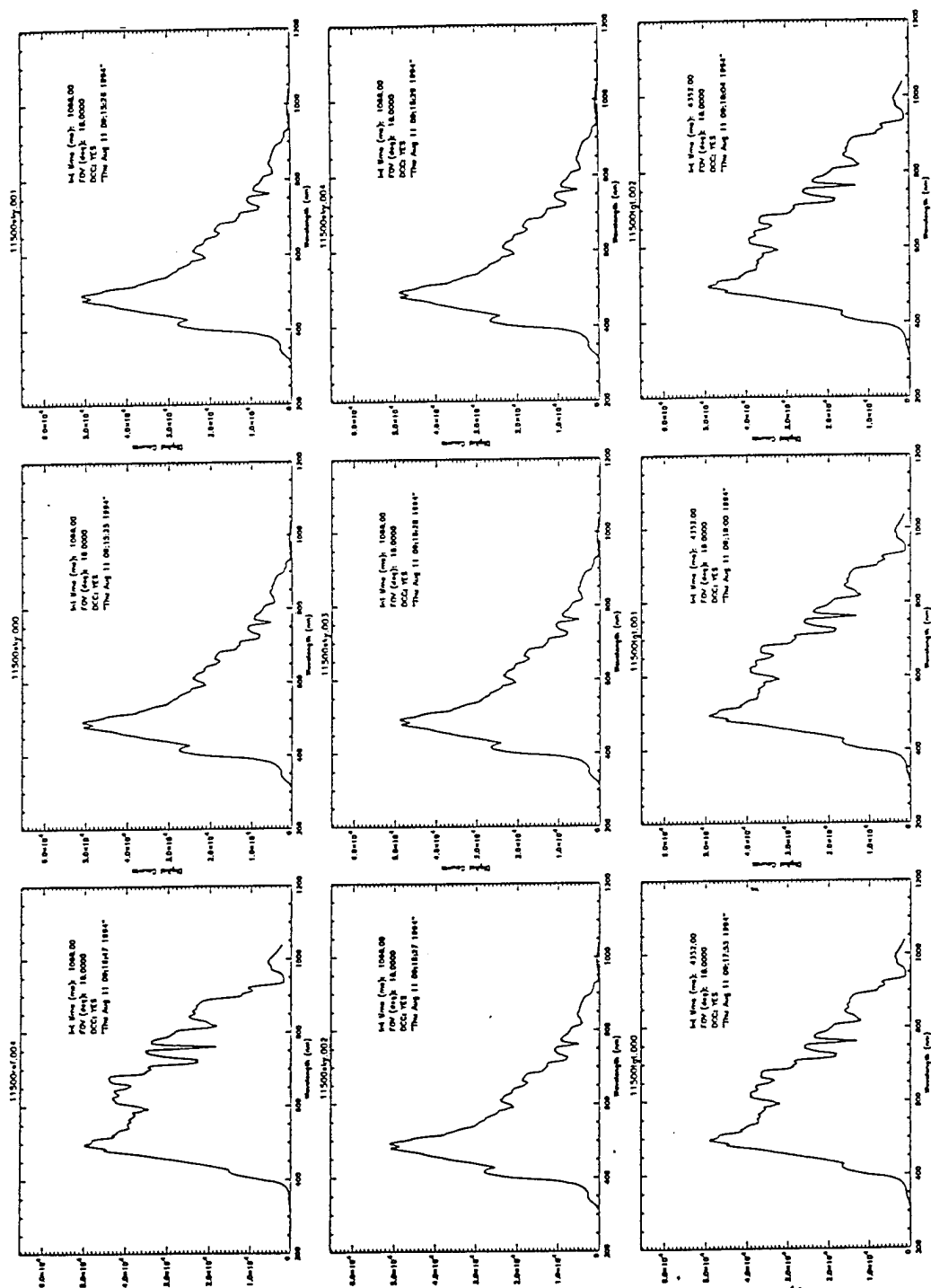


Figure 6: Example of ASD spectra hardcopy log. Each plot includes plot of spectra, integration time, FOV, dark current correction flag, and time and date spectra was saved.

$S_{w+s}$  is the spectra from the water plus reflected skylight,  $S_s$  is the spectra from the skylight,  $S_g$  is from the known reference standard,  $r_g$  is the reflectance of the reference,  $\rho(\theta)$  is the Fresnel reflectance of seawater ( $\rho(\theta) = 0.021$ ). The reflectance of land targets is computed using

$$R_t = \frac{S_t}{S_g} r_g, \quad (16)$$

where  $S_t$  is the spectra of the target. Equations (15) and (16) relaxes the necessity of absolute radiance calibration of the ASD instruments.

When spectra from both instruments were needed to compute  $R_{rs}$ , all of the spectra were converted to a common bandset, using linear interpolation, prior to using Equation (15). This step is necessary for accurate results because the two ASD instruments had different spectral response. The initial wavelength for instrument 701 (ASD701) was 331nm with a bandwidth of 1.4195nm. The initial wavelength for instrument 702 (ASD702) was 313 nm with a 1.416nm bandwidth. The difference in spectral response becomes apparent when each instrument is viewing a target simultaneously. As an illustration, Figure 7 shows the raw spectra of one of the plywood targets measured by each instrument.

All of the CASI data was provided in ERDAS LAN band interleaved by line (BIL) format. The CASI data needed to be converted to reflectance so that comparisons to the ASD measurements could be made. In regard to the CASI data, only upwelling radiance ( $L_w$ ) is known in Equation (4). Therefore,  $E_d$  must be computed in some manner since no measurement of it was made. This was accomplished by first using the reflectance of a

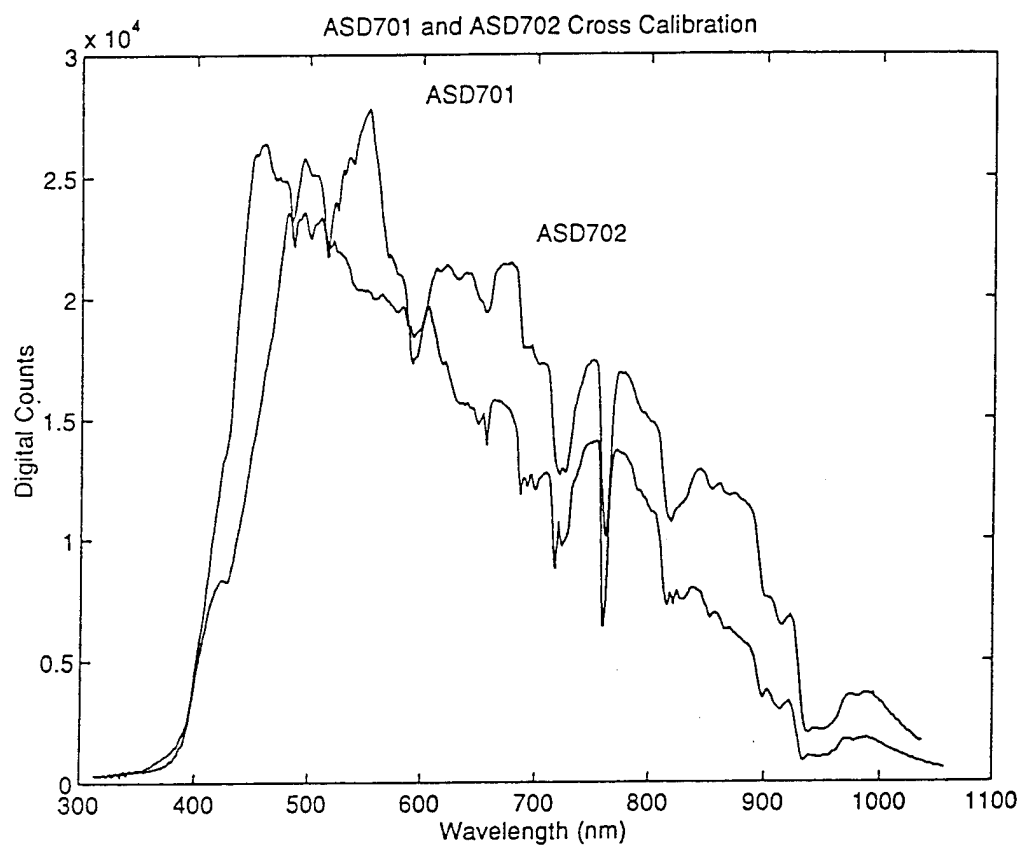


Figure 7: Raw spectra of a plywood target, measured simultaneously by both ASD instruments, illustrating the difference in spectral response of the two sensors.

land target visible in the CASI scene, measured by the ASD instruments, and using this result to compute  $E_d$  at that location. Assuming that  $E_d$  was constant throughout the image,  $R_{rs}$  was computed for the rest of the pixels in the image. This processing step also removes any atmospheric effects from the CASI imagery. It is also assumed that the atmospheric conditions are constant throughout the scene.

The principal components analysis (PCA) technique was applied to deep-to-shallow transects from both ASD and CASI spectral data. The goal of this processing step was to reduce the dimensionality of the spectral data (i.e. number of bands) yet maintain the variance of the data. As described in Chapter 2, this technique requires computation of the covariance matrix. The size of the covariance matrix is  $n$  by  $n$ , where  $n$  is the number of bands. For the ASD data,  $n = 512$ , while for the CASI data,  $n = 288$ . It is quite apparent that the size of the covariance matrix is quite large and uses quite a bit of memory. In order to reduce the memory requirements, both the ASD and CASI datasets were reduced to 64 bands each, 400 nm to 800 nm, with 8nm bandwidths, using linear interpolation.

## Chapter 4

### Results

This chapter will present the results from the analysis of the hyperspectral data collected during the Eglin field exercises. The comparison of CASI  $R_{rs}$  to ASD measured  $R_{rs}$  are the primary results. The full suite of *in-situ* measurements needed to make full use of the model described by Lee et al. [4] were not made during these exercises. Although water absorption, scattering, and diffuse attenuation coefficient were measured during the experiment, the data was not available yet for comparison with the spectral data presented in this paper.

Figure 8 is an overview of the Eglin test site as seen from a CASI spatial mode image. The sand bar running parallel to the beach is the only significant underwater feature that is visible. The land areas are comprised mainly of bright, white sand mixed with patches of vegetation. The depth of the water at the sand bar is approximately 2m. The bottom, which consists primarily of sand, has a gradual slope. The bathymetry, shown in Figure 9, was collected by the Army Corps of Engineers' SHOALS system.

ASD water spectra were measured at several preselected stations, indicated by Table 2, as well as along deep-to-shallow transects. The deepest ASD station was in approximately 10m of water. ASD spectra were also collected on land along the beach and in the surrounding area near roads and parking lots. The types of land targets included sand, sea oats, grass, concrete, and asphalt. In addition to the water



Figure 8: Overview of Eglin test site from a CASI spatial mode image. Georeferencing caused the no data area around the image.

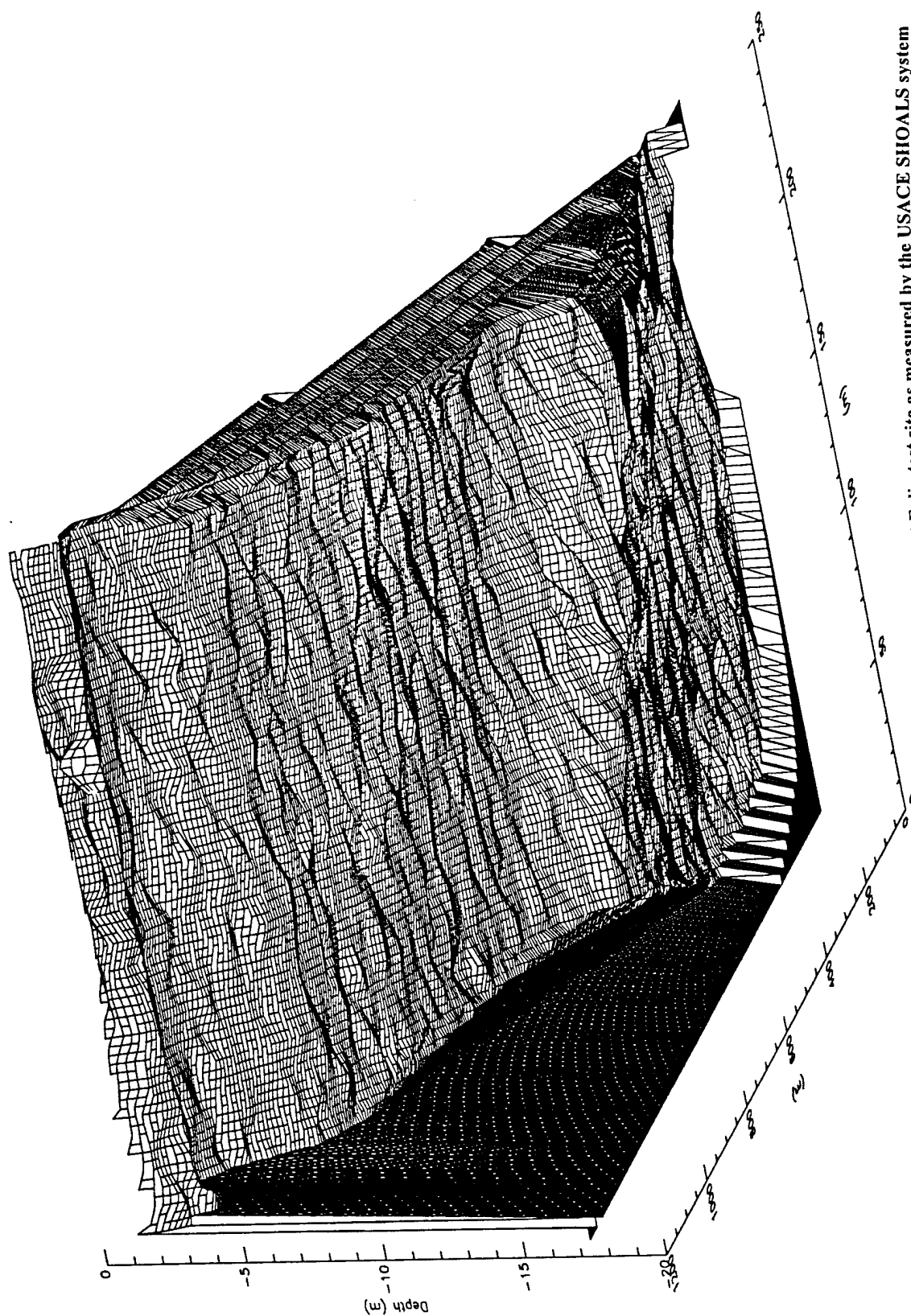


Figure 9: Bathymetry at Eglin test site as measured by the USACE SHOALS system

measurements, spectra of an underwater target and algae were also made. No accurate positioning of the ASD measurements is available.

Station #	Name	Water Depth
1	Sand Bar	3m
2	Shallow Plywood	5m
3	Shallow Mooring	3.3m
4	Deep Mooring	8.5m

Table 2: The ASD stations and the approximate water depth.

Every object or feature has a unique spectral signature based on its chemical or physical makeup. Figure 10 shows sample spectral signatures of sand, grass, algae, and water measured using the ASD instrument. Differences between the raw sample spectra are readily visible, however, spectra are typically represented in terms of radiance ( $\text{W m}^{-2} \text{sr}^{-1} \text{nm}^{-1}$ ) or reflectance. The ASD instruments were not calibrated to produce actual radiance values, therefore, the spectra in Figure 10 were converted to reflectances as shown in Figure 11 using the method described in Chapter 3. The reflectance signatures clearly illustrate the wide range in reflectance that may be encountered in the coastal environment and that each feature exhibits a unique signature. The grass and algae signatures are similar as expected. Notice that the reflectance of the land targets are much greater than the water reflectance.

In comparison, Figure 12 shows the spectral signatures of deep water, water at the sandbar, and vegetation, expressed in terms of radiance, extracted from a CASI spectral mode image. Converting the CASI spectra to reflectance requires knowledge of either downwelling irradiance ( $E_d$ ), or the reflectance of a target that is visible in the imagery.



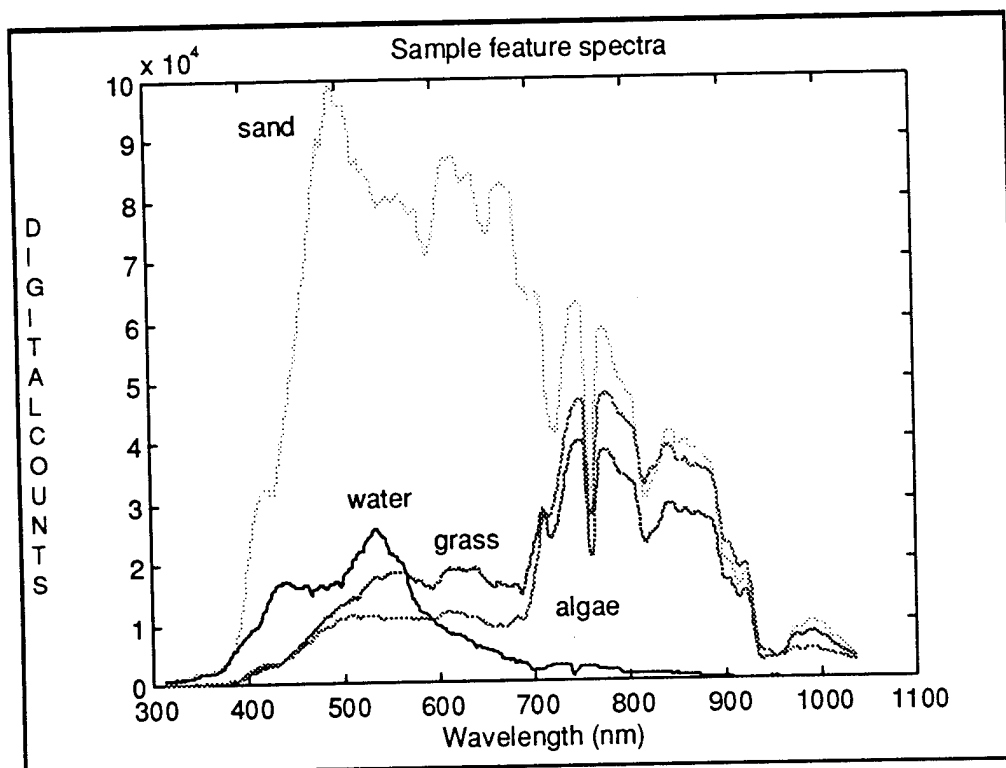


Figure 10: Raw sample feature spectra measured by the ASD instrument.

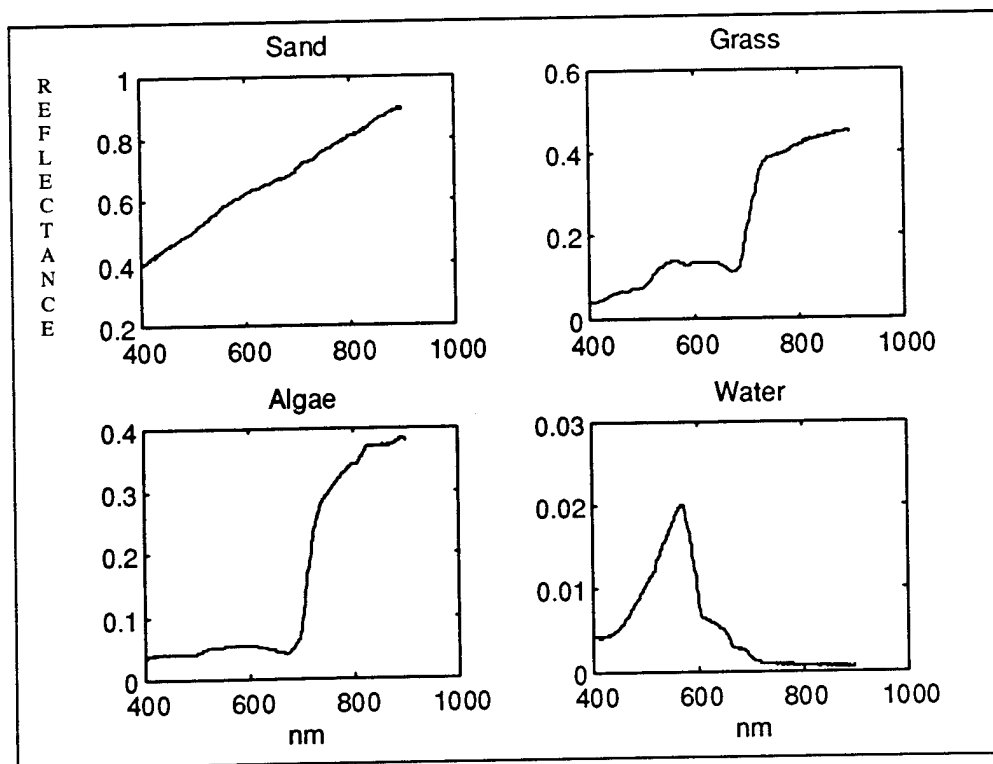


Figure 11: Reflectance spectra of sample features measured by the ASD instrument.

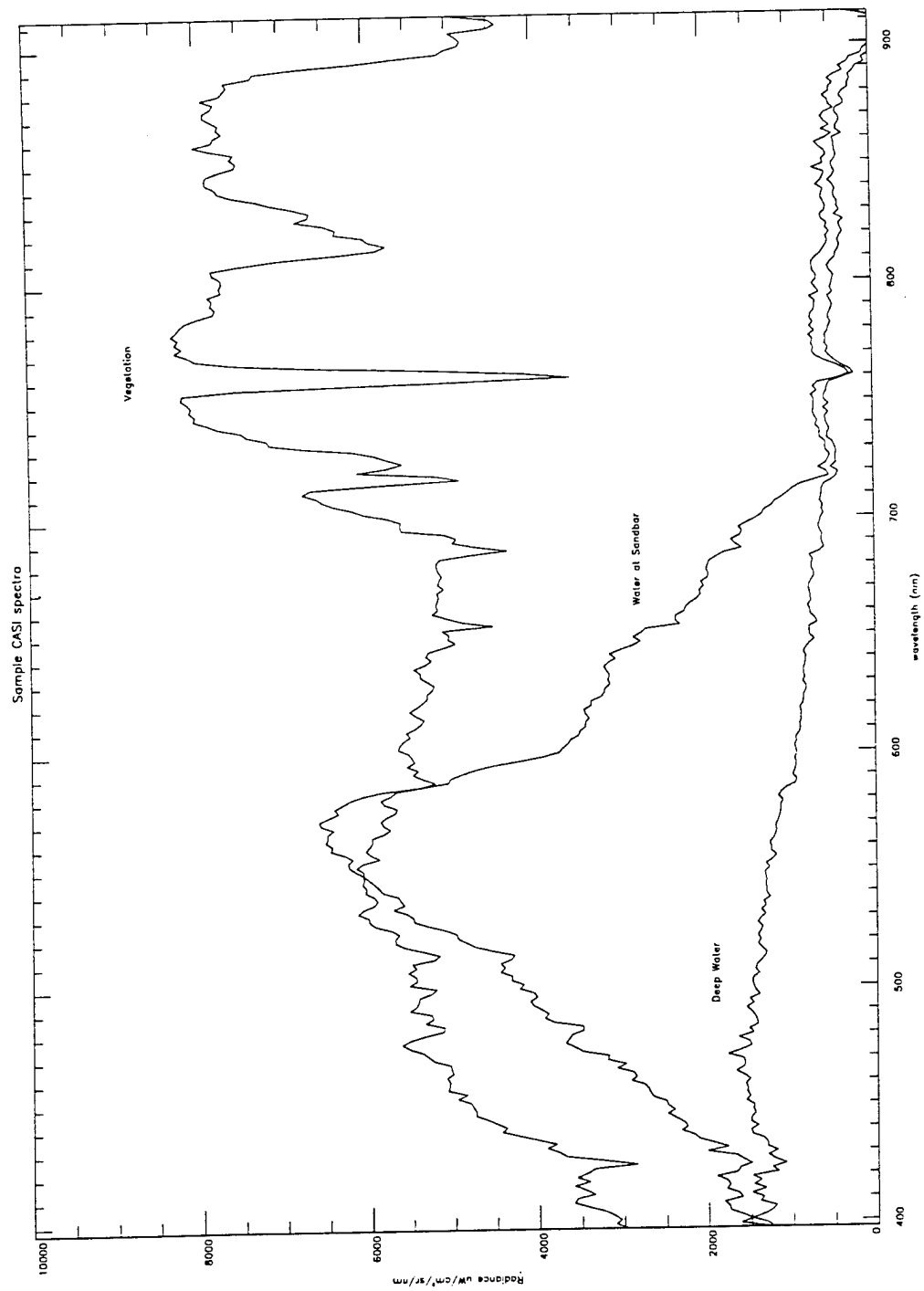


Figure 12: Spectral radiance curves for vegetation, deep water, and water at the sandbar extracted from a CASI spectral mode image.

Since no measurements of  $E_d$  were made, a reference target of known reflectance must be located in the imagery. Figure 13 is the track recovery row image from a CASI spectral mode image. As this figure illustrates, it is quite difficult to locate specific targets from a CASI spectral mode image. This image has no roll, or pitch corrections applied to it nor has it been georeferenced. Because of the difficulties with selecting a reference target from the track recovery row images no direct comparisons with ASD spectra will be presented. Plywood targets, which were placed out in the water to serve as reference targets for the CASI imagery, although visible in the spatial imagery, proved to be too small to serve as references. The plywood pixels are at best 1 pixel in size and, due to the spatial resampling of the imagery to create square pixels, the plywood pixel is a mixture of both water and plywood.

Figure 14 shows  $R_{rs}$  computed, from the ASD data, at the shallow plywood and deep mooring stations on August 9. The amplitude difference between the two spectra and the peak at about 560 nm are related to the increasing effects of the bottom reflectance from the sandy bottom. An ASD deep-to-shallow transect measured on August 11, shown in Figure 15, clearly shows the significant increase reflectance centered around 560 nm. The spectra where the peak of the reflectance occurs was measured at the sand bar.

Comparing the ASD measured  $R_{rs}$  to the CASI data required converting the CASI radiance data to reflectance.  $E_d$ , computed at one location in the CASI scene, was determined from Equation (4) by using the reflectance of a land target visible in the imagery. The reflectance of an asphalt road, measured by the ASD, and visible in the

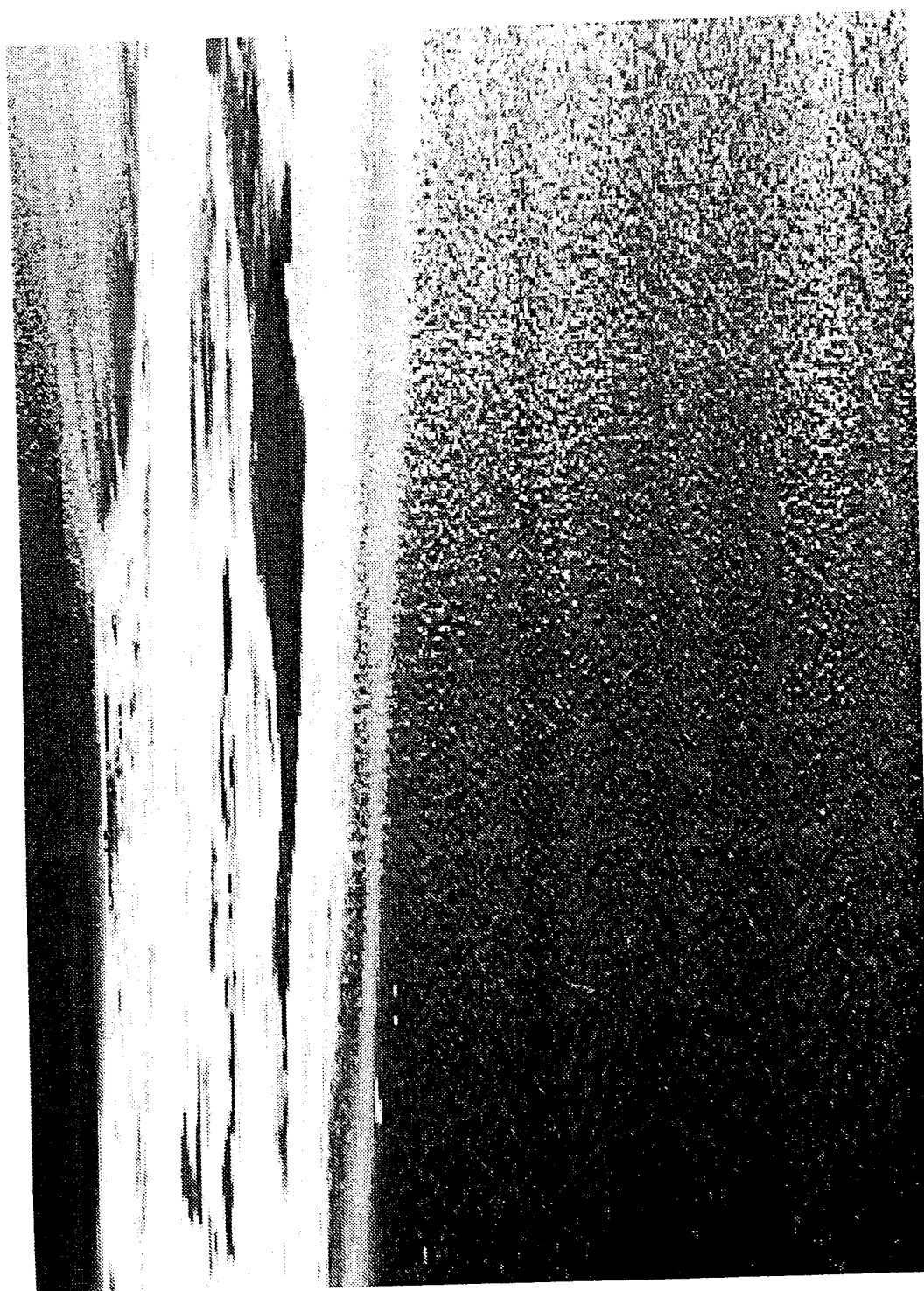


Figure 13: CASI spectral mode track recovery row image.

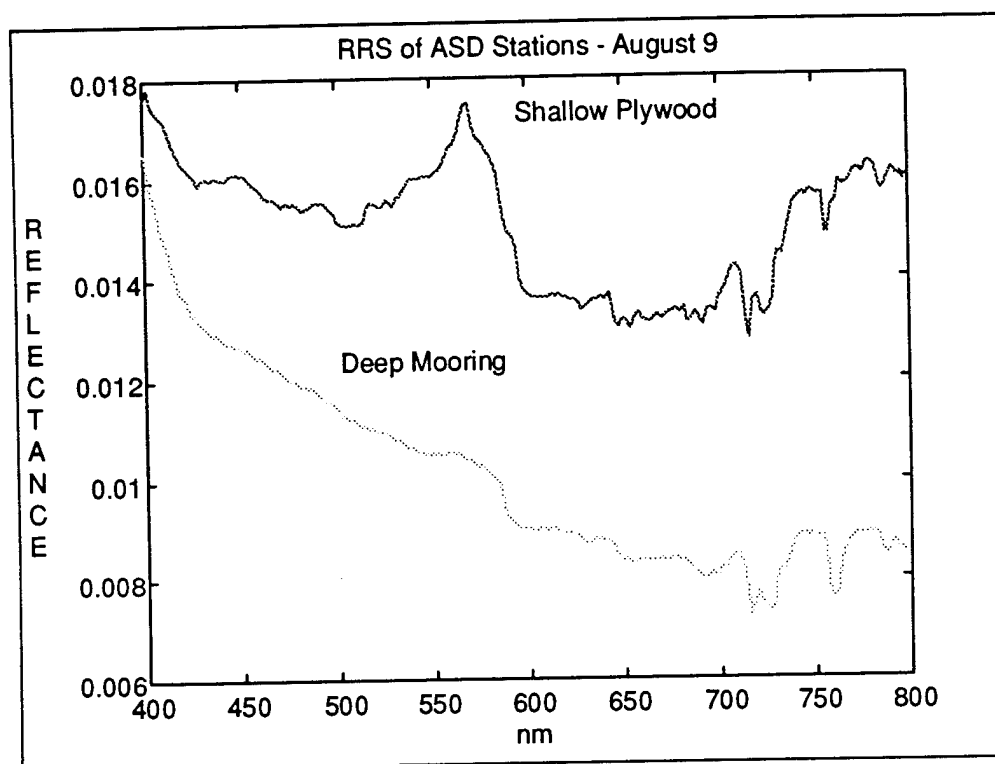


Figure 14:  $R_{rs}$  measured using the ASD instrument at the shallow plywood and deep mooring stations on August 9.



Figure 15:  $R_n$  of August 11 ASD deep-to-shallow transect spectra.

CASI spatial mode imagery, was used as the reference. The beach sand was not used as the reference, although ASD measurements were made of the sand, because of detector saturation of the CASI. The asphalt road was chosen since it appears to be considerably darker than the sand. Saturation of the beach sand was also another reason why the sand was not used as a reference for the CASI spectral mode data.

Figure 16 shows  $R_{rs}$ , computed along a deep-to-shallow transect extracted from a CASI spatial mode image, for five of the eleven bands. The sand bar is located approximately between spectra 300 and spectra 360. Figure 17 shows  $R_{rs}$  computed for the August 11 ASD transect data for the same CASI bands in Figure 16. The areal coverage between the two transects is not exact, however, the results are quite good. Note that the CASI values are slightly higher than the ASD values, however, the CASI pixels cover a larger area than the ASD measurement, which may account for some of the difference. In either case, reflectance increases with decreasing water depth. For the spectral range shown, reflectance also increases with wavelength for both datasets. Figure 18 shows a deep-to-shallow transect extracted from an August 10 CASI spatial image. No ASD transect data is available for August 10, however, the results are comparable to the August 11 data, except for the unusually high values at 554 nm. The CASI August 10 results suggest that there appears to be some variability in the water reflectance from day-to-day since these values are a bit lower than those on August 11. An examination of the water absorption and scattering are needed to verify this result. Spatial differences can also be a factor in the difference in reflectance, especially since the CASI transects from August 10 and 11 were not extracted from the exact same location.

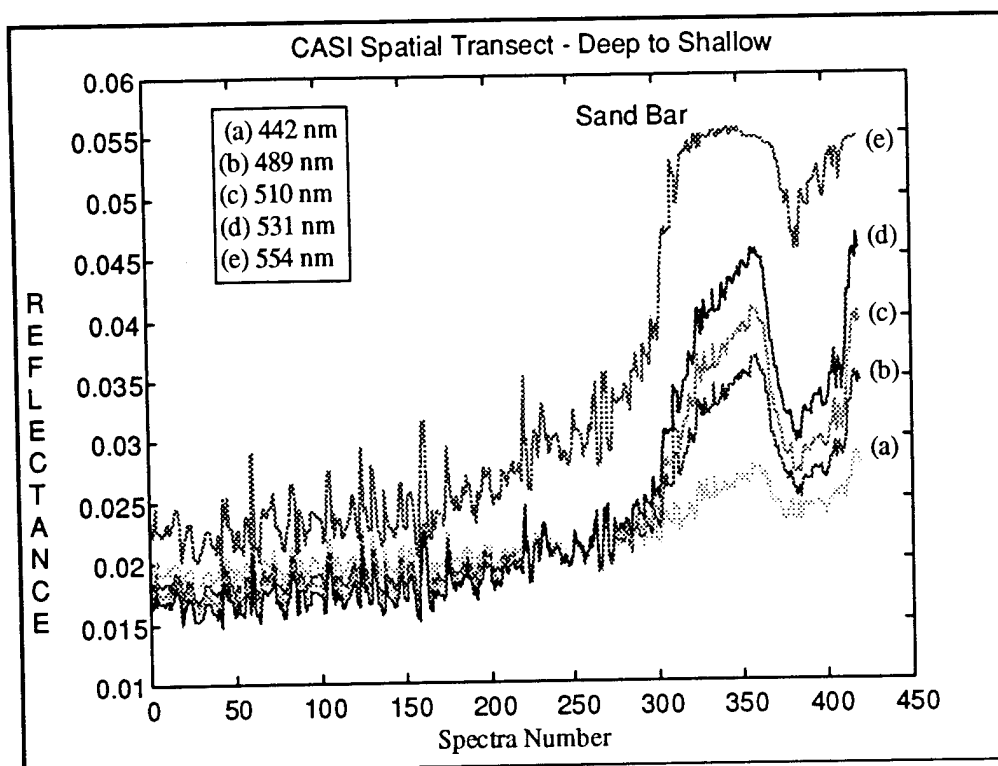


Figure 16: Transect extracted from 11AUGF24T1 that ranges from the deeper water to the shallow water.

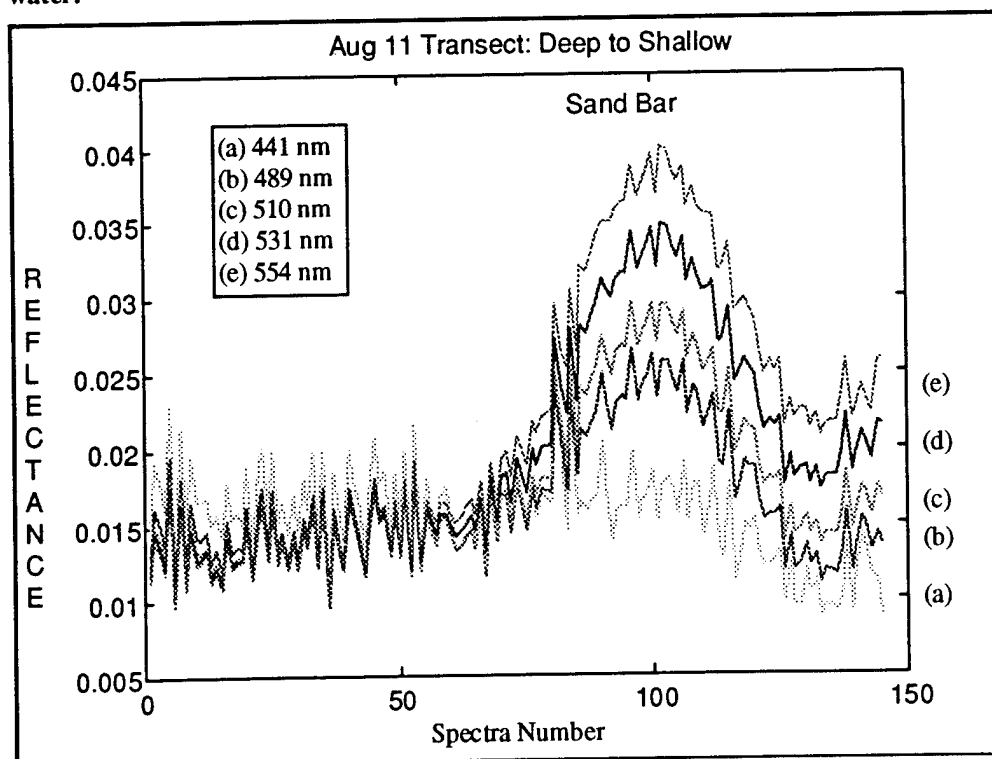


Figure 17: Remote Sensing Reflectance for Aug 11 ASD transect. The wavelengths correspond to the wavelengths associated with the CASI spatial file 11augf24t1.lan.



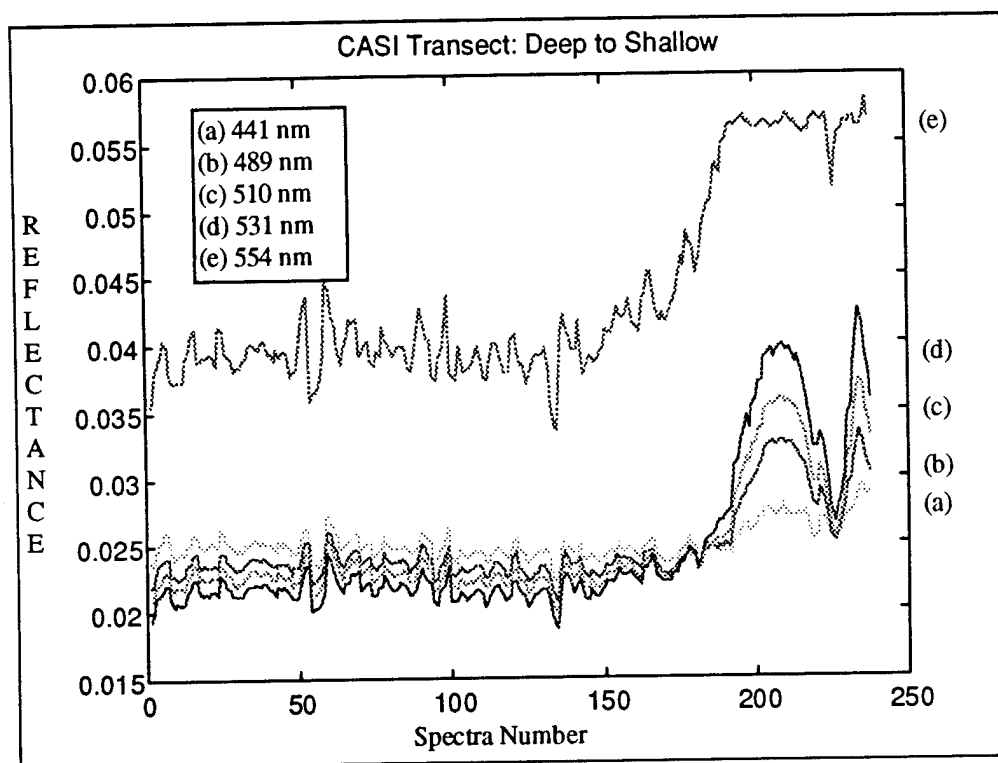


Figure 18: Transect extracted from 10augf21t1 and ranges from the deep to the shallow.

As mentioned in Chapter 3, PCA was applied water spectra from both ASD and CASI spectral mode data in an attempt to reduce the dimensionality (i.e. number of bands) of the data. To reduce the memory requirements of the computer performing the analysis, both datasets were first reduced to 64 bands using linear interpolation, ranging from 400 nm to 912 nm. In both cases, the first two principal components (PCPs) accounted for more than 95% of the variation in the data, with at least 80% associated with PCP1. The first three eigenvectors associated with the ASD transect data are shown in Figure 19. The associated PCPs are shown in Figure 20. Figure 21 shows the first three eigenvectors from a sample CASI dataset. Notice that the shape of the PCP1 for the ASD data resembles the shape of the reflectance curve shown in Figure 17. This result indicates that PCP1 is related to brightness, which is related to changes in bathymetry. The fact that PCP1 is correlated with brightness is not an uncommon result for this type of data, as pointed out by Gonzalez [21]. PCP2 has an intriguing result due to the significant dip in the curve after spectra 100. Spectra 100 is the location of the sandbar. One might speculate that PCP2 may be related to changes in water turbidity, which would be a most useful result. Notice also that the eigenvectors from both datasets have similar shapes. PCA certainly reduces the dimensionality of the spectral data, however, the relationship between the PCPs, other than PCP1, and some property of the spectral data is not obvious. Further research in this area is certainly warranted.

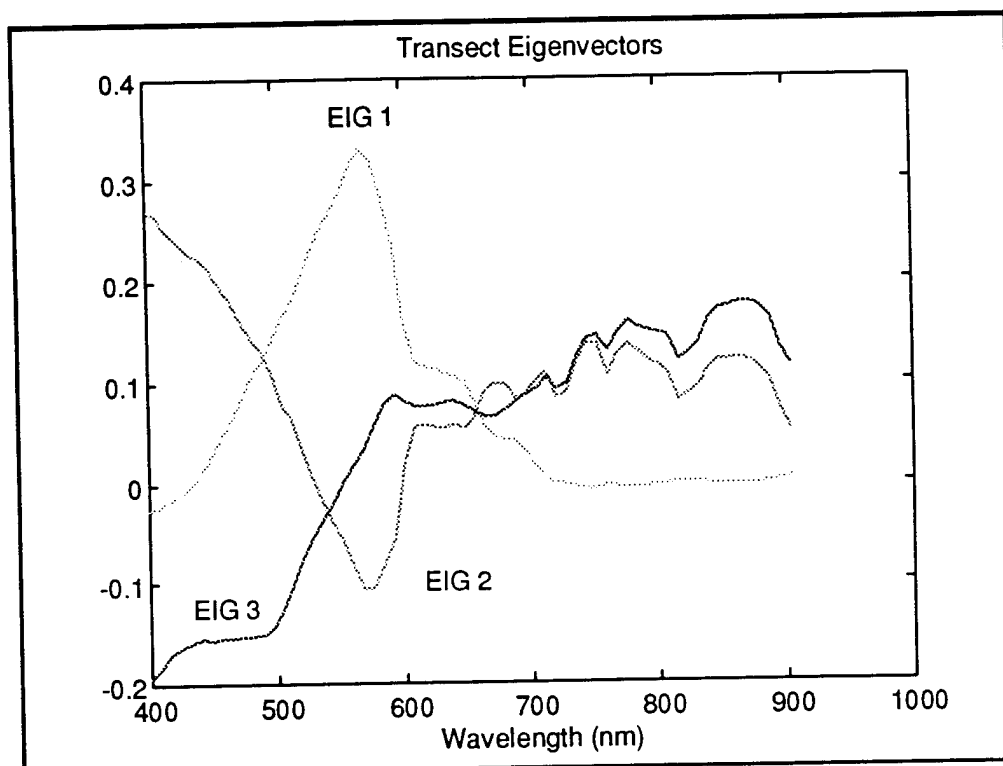


Figure 19: PCA using the August 11 ASD transect spectra. The first three eigenvectors are shown.

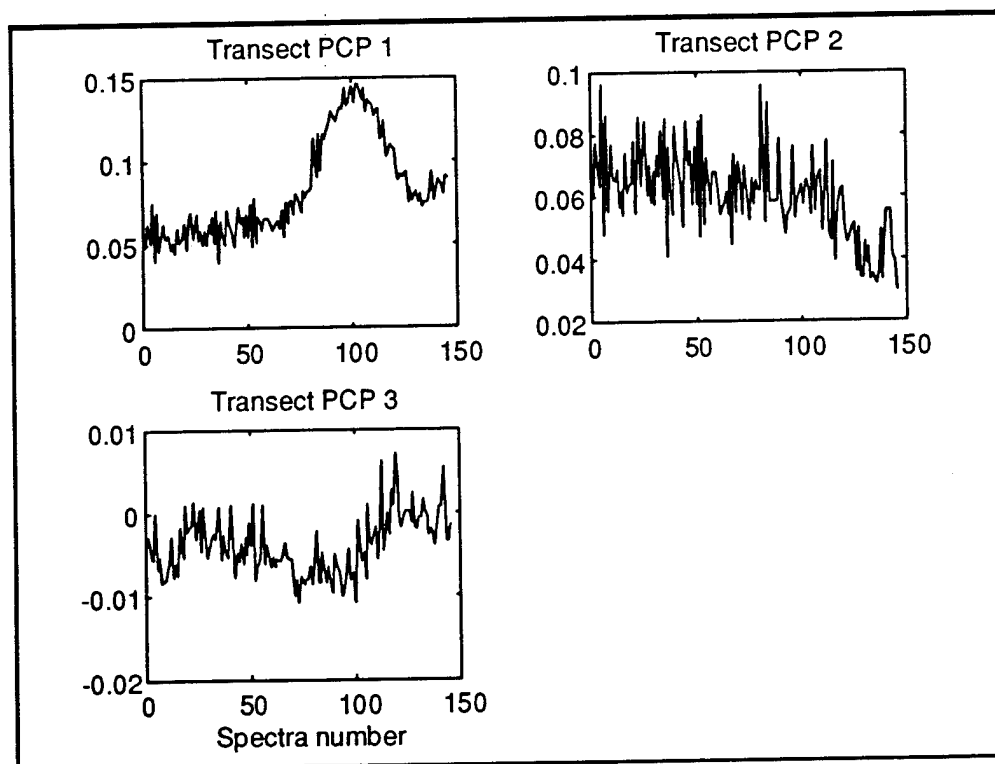


Figure 20: The first three PCP computed from the August 11 ASD transect spectra.

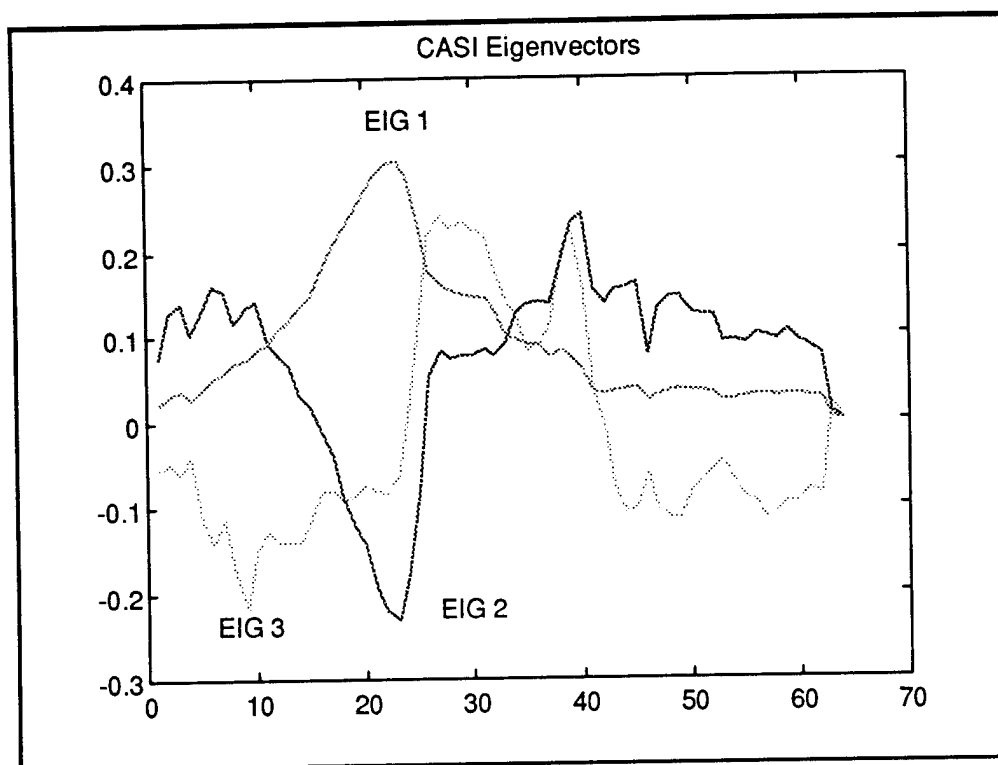


Figure 21: Sample CASI Eigenvectors

## Chapter 5

### Conclusions and Recommendations

The results from the Eglin field experiment demonstrate that hyperspectral data can be used to distinguish between both land and water features. Also, remote sensing reflectance of the water derived from the CASI HSI sensor agrees reasonably well with *in-situ* measurements from ASD instruments, and is within the expected range. PCA of both the CASI and ASD data indicate that the 95% of the variance is contained in the first two PCPs. Although the PCA results are not completely understood, further research is needed.

It is apparent that HSI sensors will play an important role in the understanding of biological and physical processes in the coastal maritime environment. Increased understanding of this complex environment will lead to the development of more accurate prediction models for chlorophyll concentration, water turbidity, particulate and biological absorption and scattering, bathymetry, bottom reflectance, etc.

Support from DOD for coastal environmental research has increased significantly since the end of the Cold War in order to support regional conflict scenarios. Civilian research has increased too, due to continued emphasis in monitoring man's effect on the ocean environment, in particular, and the global environment as a whole. Remote sensing instruments provide the fastest and most cost effective method of collecting high

resolution data. At this juncture, no spaceborne HSI sensors exist, however, the number of airborne sensors are continuing to rise.

One of the major issues concerning the use of current HSI sensors in the maritime environment is the SNR in the blue portion of the spectrum. Adequate SNR is required because the reflectance of water features tend to be significantly smaller than land features. Furthermore, due to the physics of light in water, the variability of water spectra is limited to the 400nm to 700nm range. SNR can be increased using spatial averaging, however, this is undesirable because of the loss of spatial resolution. SNR performance criteria for sensors that will be used for maritime use must be taken in consideration.

To date, none of the current HSI instruments has been designed exclusively for maritime applications. It may seem impractical to design a high resolution device just for oceanographic work when most of the research is limited to the 400nm to 700nm range. However, coastal environments typically are a combination of both land and water features, therefore the HSI instrument must have adequate SNR and dynamic range to be able to discern between features. In order to obtain satisfactory data over both land and water, there is a need for a dual sensor suite consisting of one optimized for land use and one optimized for ocean use. In the meantime, a more detailed investigation of the capabilities of the HSI sensors summarized by Birk and McCord [17] would be worthwhile. The results of this study would identify the sensors that are best suited for collecting data in the maritime environment.

Although the CASI reflectance results agreed reasonably well with the ground truth data, improvements to the sensor would greatly enhance its usability. The major

drawback with using the CASI is that full spectral and spatial data over the entire scene is not available simultaneously. Loss of data results in the spectral mode due to the spacing between the look directions across the detector array and it is very difficult if not impossible to identify targets or features in the track recovery row image since it is not geometrically corrected. Fixing this problem, though, would most certainly drive up the cost of operating the CASI. Its low cost of operation, as well as, high spatial resolution, and adaptability to various aircraft platforms are its major selling points. SNR and dynamic range also needs to be improved so as to better accommodate both water and land features.

The ASD instruments proved to be quite useful tools in the coastal environment. The instruments need to be ruggedized for the harsh environmental conditions associated with field work. In particular, a water-proof design is highly recommended for use near water.

The modeling community is in need of high resolution spatial and spectral data for the development of coastal optics models. The models used in this paper are still under development. Adequate ground truthing is still needed in order to validate the results derived from the imagery. Instruments of the ASD genre will greatly aid in the collection of the necessary *in-situ* measurements, but radiometric calibration of these instruments is highly recommended especially if the data is to be compared to calibrated HSI data. The SNR performance of the ASD instruments also needs to be evaluated. Integration of precise positioning information using differential GPS is highly recommended for the ASD instruments.

High resolution spectral instruments have more than enough spectral coverage in the visible portion of the spectrum. The PCA results in Chapter 4 showed that water spectra contains a considerable amount of redundancy, thus PCA can certainly be used as a data compression scheme. PCA could also be used as a coastal feature identification technique in the same vein as the work performed by Huerte and Escadafal [19] for soil identification. The spectral signatures of different bottom types, sand, vegetation, water turbidity, chlorophyll concentration, etc. could be combined into a database as endmember spectra. Spectral unmixing techniques could be used to identify the desired component spectra at each pixel in the hyperspectral image.

The use of HSI sensors for remote sensing of the environment has a bright future. Airborne systems will be utilized until sensor technology improves to the state where spaceborne systems are practical. Shrinking budgets in both the private and public sectors will require sharing of resources, which means that remote sensing instruments will most likely be designed for use in a variety of applications.



## References

1. Jerlov, N. G., *Optical Oceanography*, Elsevier, New York, 1968.
2. Tyler, J. *Light in the Sea*, Dowden, Hutchinson, & Ross, Stroudsburg, PA, 1977.
3. Gordon, H.R. and D.K. Clark, "Clear water radiances for atmospheric correction of coastal zone color scanner imagery," *Applied Optics*. Vol. 20, No. 24, pp. 4175-4180, 1981.
4. Lee, Z., K.L. Carder, S.K. Hawes, R.G. Steward, T.G. Peacock, and C.O. Davis, "A model for interpretation of hyperspectral remote-sensing reflectance," in publication.
5. Hovis, W.A. Clark, D.K., Anderson, F. et al. "Nimbus-7 coastal zone color scanner; system description and initial imagery. *Science* 210:60-63, 1980.
6. Gordon, H., Clark, D., Brown, J., Brown, O., Evans, R., and Brokenow, W., "Phytoplankton pigment concentrations in the Middle Atlantic Bight: comparison of ship determinations and CZCS estimates," *Applied Optics* 22(1):20-36, 1983.
7. Austin, R.W. and Petzold, T.J. "The determination of the diffuse attenuation coefficient of sea water using the Coastal Zone Color Scanner," *Oceanography from Space*. pp 239-256, 1981.
8. Arnone, R.A., Oriol, R.A., Terrie, G.E., and Estep, L. "Optics Database," NRL Technical Note 254, 1992.
9. Lyzenga, D.R., "Passive remote sensing techniques for mapping water depth and bottom features," *Applied Optics*, Vol. 17, No. 3, pp. 379-383, 1978.
10. Polcyn, F.C. W.L. Brown, and I.J. Sattinger, "The measurement of water depth by remote sensing techniques," Report 8973-26-F, Willow Run Laboratories, U. Michigan, Ann Arbor, 1970.
11. Clark, R.K., T.H. Fay, H.V. Miller, and C.L. Walker, "Bathymetry calculations with LANDSAT 4 Thematic Mapper under a generalized ratio assumption," *Applied Optics*, Vol. 26, No. 19, pp. 4036-38, 1987.
12. Mertes, L. "Rates of flood-plain sedimentation on the central Amazon River," *Geology*, v. 22, pp. 171-174, February 1994.
13. Mertes, L., Smith, M., and Adams, J. "Estimating suspended sediment concentrations in surface waters of the Amazon River wetlands from LANDSAT images," *Remote Sensing Environment* 43:281-301, 1993.
14. Carder, K.L., P. Reinersman, R.F. Chen, F. Muller-Karger, C.O. Davis, and M. Hamilton, "AVIRIS calibration and application in coastal oceanic environments," *Remote Sens. Environ.* 44:205-216 (1993).

15. Hamilton, M.K, C.O. Davis, W.J. Rhea, S.H. Pilorz, and K.L. Carder, "Estimating chlorophyll content and bathymetry of Lake Tahoe using AVIRIS data," *Remote Sens. Environ.* 44:217-230 (1993).
16. Pilorz, S.H., Davis, C.O., "Spectral decomposition of ocean reflectance with AVIRIS data," in *Proceeding of the Second Airborne Visible/Infrared Imaging Spectrometer Workshop*, JPL Publication 90-54, Pasadena, CA, pp. 224-231, 1990.
17. Birk, R.J. and McCord, T.B., "Airborne Hyperspectral Sensor Systems," *IEEE AES Magazine*, pp. 26-33, October 1994.
18. Kruse, F.A., Lefkoff, A.B., and Dietz, J.B., "Expert system-based mineral mapping in Northern Death Valley, California/Nevada, using the Airborne Visible/Infrared Imaging Spectrometer (AVIRIS)," *Remote Sens. Environ.*, 44:309-336, 1993.
19. Huete, A.R. and R. Escadafal, "Assessment of biophysical soil properties through spectral decomposition techniques," *Remote Sens. Environ.*, 35:149-159, 1991.
20. Estep, L. "Spectral principal components of the upwelling light field from the ocean surface," *Proceedings SPIE Optics of the Air-Sea Interface*, Vol. 1749, 1992.
21. Gonzalez, R.C., Woods, R.E. *Digital Image Processing*. Addison-Wesley, Reading, MA 1992.
22. Jolliffe, I.T. *Principal Component Analysis*. Springer-Verlag, New York 1986.

## Biography

Gregory E. Terrie was born on June 9, 1964, in Wichita Falls, Texas. He received a B.S. degree in Electrical Engineering from the University of New Orleans in 1988 and a B.A. degree from Xavier University of Louisiana in 1989. He entered the Tulane Engineering Graduate School in September 1993. He is currently employed by the Naval Research Laboratory at Stennis Space Center in Mississippi where he serves as an Electronics Engineer in the Mapping, Charting, and Geodesy Branch. During his tenure at NRL, his research and development efforts have been focused on extracting environmental information from remote sensing instruments such as, satellite and airborne imaging sensors, lasers, and airborne electromagnetometers. He is currently a member of IEEE and SPIE.